Journal of Solid State Chemistry 183 (2010) 2974–2978

Contents lists available at ScienceDirect

Journal of Solid State Chemistry

journal homepage: www.elsevier.com/locate/jssc

Preparation and structural study from neutron diffraction data of $Pr_5Mo_3O_{16}$

M.J. Martínez-Lope [a], J.A. Alonso [a,*], D. Sheptyakov [b], V. Pomjakushin [b]

[a] Instituto de Ciencia de Materiales de Madrid, C.S.I.C., Cantoblanco, E-28049 Madrid, Spain.
[b] Laboratory for Neutron Scattering, Paul Scherrer Institut, CH-5232 Villigen PSI, Switzerland

ARTICLE INFO

Article history:
Received 17 September 2010
Accepted 12 October 2010
Available online 20 October 2010

Keywords:
R_2MoO_6
Rare-earth molybdenum oxides
Fluorite superstructure
Mixed valence compound
Ce_2MoO_6
$Ce_5Mo_3O_{16}$

ABSTRACT

The title compound has been prepared as polycrystalline powder by thermal treatments of mixtures of Pr_6O_{11} and MoO_2 in air. In the literature, an oxide with a composition Pr_2MoO_6 has been formerly described to present interesting catalytic properties, but its true stoichiometry and crystal structure are reported here for the first time. It is cubic, isostructural with $CdTm_4Mo_3O_{16}$ (space group *Pn*-3*n*, $Z=8$), with $a=11.0897(1)$ Å. The structure contains MoO_4 tetrahedral units, with Mo–O distances of 1.788(2) Å, fully long-range ordered with PrO_8 polyhedra; in fact it can be considered as a superstructure of fluorite (M_8O_{16}), containing 32 MO_2 fluorite formulae per unit cell, with a lattice parameter related to that of cubic fluorite ($a_f=5.5$ Å) as $a \approx 2a_f$. A bond valence study indicates that Mo exhibits a mixed oxidation state between 5+ and 6+ (perhaps accounting for the excellent catalytic properties). One kind of Pr atoms is trivalent whereas the second presents a mixed Pr^{3+}–Pr^{4+} oxidation state. The similarity of the XRD pattern with that published for Ce_2MoO_6 suggests that this compound also belongs to the same structural type, with an actual stoichiometry $Ce_5Mo_3O_{16}$.

1. Introduction

Metal oxides simultaneously containing transition metals and lanthanide ions present a panoply of interesting properties and applications, spanning from superconductivity (e.g. in (La,Sr)$CuO_{4-\delta}$) [1] to colossal magnetoresistance (e.g. in (La,Ca)MnO_3) [2] or catalysis (e.g. $CaFeO_{3-\delta}$) [3]. When both metal ions posses a variable oxidation state, the prospect of charge transfer between them appears as an attractive possibility, perhaps associated with novel phenomena and functionalities. As a requirement, the chemical potential of the *f* ion should be energetically close to the Fermi level of the transition-metal *d*-bands [4]. This circumstance is accomplished when the *f* ion is a light lanthanide, particularly Ce or Pr, where the *f* orbitals are extended and available for bonding. Selective catalytic activity has been described among these kind of materials [5,6].

Within the field of heterogeneous catalysis, particularly appealing are the ternary Pr–Mo–O [7] and quaternary Bi–Pr–Mo–O [8–10] phases, which are active as catalysts for the partial oxidation of propene and isobutene. An oxide named Pr_2MoO_6 is present in the phase diagram of the Pr–Mo–O system and participates in the catalytic activity for selective olefin oxidation [11–13]. This Pr_2MoO_6 oxide has also been reported among the other members of the well-described R_2MoO_6 family (R=rare earths) [14]. Depending on the size or the synthetic conditions, R_2MoO_6 compounds have been described to crystallize in three polymorphs, with monoclinic (α), cubic (β) and tetragonal (γ) symmetries [14]. Most of the small-sized rare-earth cations form the monoclinic (α) phase, which is closely related to the scheelite-type structure. Scheelite itself is a superstructure of fluorite (CaF_2, cubic, $a=5.5544$ Å, *Fd*-3*m*) [15]. The crystal structure of the α-phase has been recently refined for Tb_2MoO_6 in the *I*2/*c* space group from neutron powder diffraction data [14], as well as those of the remaining α-R_2MoO_6 polymorphs for small-sized rare earths, R=*Y*, Dy, Ho, Er, Tm, Yb [16]. The La polymorph is tetragonal (space group $I4_1/acd$, γ phase) [14] whereas the Ce, Pr and Nd compounds have been described as pseudocubic (β phase) [4,14] although the space group symmetry and structural features have not been reported so far. For R=Pr, Nd it seems that the materials prefer either the pseudocubic or the tetragonal structures, depending on the synthesis conditions: the tetragonal form is the high-temperature phase, whereas the pseudocubic structure (β) can be stabilized at low temperatures [14].

In this work we have focused on the actual composition and crystal structure of the so-called Pr_2MoO_6 pseudocubic oxide. In fact it presents a stoichiometry $Pr_5Mo_3O_{16}$ and it consists of a cubic superstructure of fluorite, where a mixed or intermediate valence for Pr and/or Mo is expected from the nominal composition. Given the weak X-ray scattering power of oxygen compared to that of praseodymium or molybdenum atoms, neutron powder diffraction has been the technique of choice for this investigation. A bond-valence study was of much help to unveil the valence state for the involved metals in this oxide.

2. Experimental

A sample of nominal composition Pr_2MoO_6 was prepared by a solid state reaction from stoichiometric amounts of analytical

* Corresponding author.
E-mail address: ja.alonso@icmm.csic.es (J.A. Alonso).

0022-4596/$ - see front matter © 2010 Elsevier Inc. All rights reserved.
doi:10.1016/j.jssc.2010.10.015

grade Pr_6O_{11} and MoO_2. The reactants were mixed, ground and calcined at 1100 °C for 12 h in air.

The initial characterization of the product was carried out by laboratory X-ray diffraction (XRD) (Cu $K\alpha$, $\lambda = 1.5406$ Å). A room-temperature neutron powder diffraction (NPD) diagram was collected at the HRPT diffractometer of the SINQ spallation neutron source at PSI, with a wavelength of 1.494 Å. The high intensity mode was used; the collection time was 2 h. The structure has been solved ab-initio with the FOX [17] software. The refinement of the crystal structure was performed by the Rietveld method, using the FULLPROF refinement program [18], with the use of its internal tables for the coherent scattering lengths of corresponding elements. The peak profiles were fitted by the Thompson–Cox–Hastings pseudo-Voigt function corrected for axial divergence asymmetry. The following parameters were refined in the final run: scale factor, background coefficients, zero-point error, pseudo-Voigt corrected for asymmetry parameters, positional coordinates and anisotropic thermal factors.

3. Results and discussion

A polycrystalline oxide of nominal composition Pr_2MoO_6 was obtained as a pale yellow powder. Fig. 1 shows the corresponding XRD diagram, fitted to the structural model described below. The pattern seems to be characteristic of a fluorite-like structure (cubic, $a = 5.54$ Å). However, the NPD pattern shows many more reflections that cannot be indexed in a simple fluorite subcell, already indicating that Pr and Mo are not randomly distributed over the same crystallographic positions, but are long-range ordered in a fluorite superstructure. On the other hand, this XRD diagram is very similar to that given by Antonio et al. [4] for Ce_2MoO_6, for which the crystal structure was not reported. The superstructure reflections were more clearly visible in the NPD diagram, which was indexed with the TREOR programs in a cubic unit-cell with $a = 11.084$ Å. A pattern matching (Le Bail fit) in this unit cell leads to an excellent agreement between observed and calculated profiles. The systematic extinctions were consistent with the *Pn*-3*n* space group (No. 222). In the asymmetric unit there are two independent Pr atoms at 12*e* (x, 1/4,1/4,) and 8*c* (0,0,0) positions, Mo at 12*d* (0, 3/4,1/4) sites and the two kinds of oxygen atoms at 48*i* (x, y, z) and 16*f* (x, x, x) positions. Fig. 2 illustrates the goodness of the NPD fit. The crystallographic formula indeed corresponds to $Pr_5Mo_3O_{16}$,

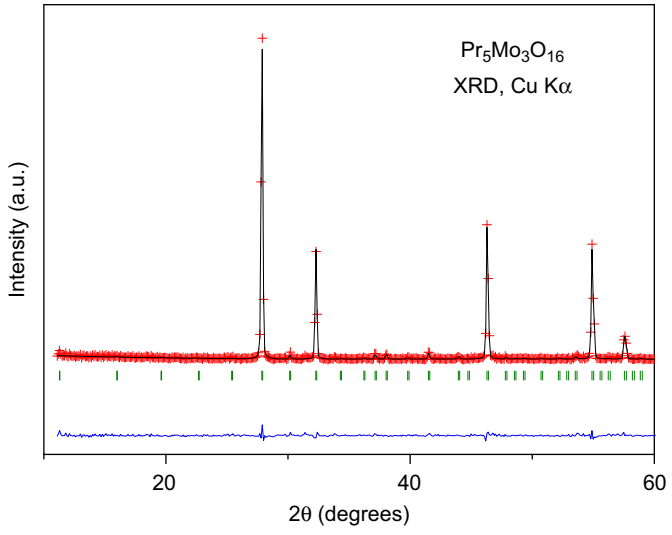

Fig. 1. XRD pattern of $Pr_5Mo_3O_{16}$. The Rietveld fit corresponds to the structural model described in the *Pn*-3*n* space group, with $a = 11.08979(9)$ Å.

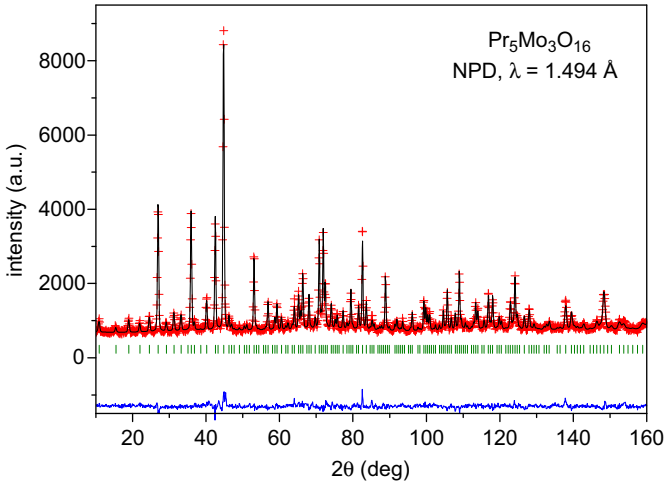

Fig. 2. Observed (crosses), calculated (solid line) and difference (at the bottom) NPD profiles for $Pr_5Mo_3O_{16}$ at 295 K. The tick marks indicate the positions of the allowed Bragg reflections.

Table 1
Structural parameters for $Pr_5Mo_3O_{15}$ refined in the cubic *Pn*-3*n* space group (No. 222) at room temperature from NPD. Lattice parameters: $a = 11.08979(9)$ Å and $V = 1363.86(2)$ Å^3. Discrepancy factors: $R_p = 3.46\%$, $R_{wp} = 4.49\%$, $R_{exp} = 3.19\%$, $\chi^2 = 1.98$ and $R_{Bragg} = 7.09\%$.

Atom	Site	x	y	z	B_{eq}(Å^2)
Pr1	12*e*	0.0089(5)	0.2500	0.2500	0.51(8)
Pr2	8*c*	0.0000	0.0000	0.0000	1.32(16)
Mo	12*d*	0.0000	0.7500	0.2500	0.98(7)
O1	48*i*	0.5851(2)	0.3629(2)	0.8275(2)	1.74(4)
O2	16*f*	0.1203(3)	0.1203(3)	0.1203(3)	0.71(4)

Atom	Anisotropic thermal factors ($\times 10^4$)					
	β_{11}	β_{22}	β_{33}	β_{12}	β_{13}	β_{23}
Pr1	4(4)	13(3)	13(3)	0	0	0
Pr2	27(3)	27(3)	27(3)	−4(3)	−4(3)	−4(3)
Mo	29(4)	16(2)	16(2)	0	0	0
O1	41(2)	23(2)	42(2)	−9(2)	17(2)	−1(2)
O2	14(1)	14(1)	14(1)	0	0	0

$Z = 4$. In fact, this structural arrangement resulted to be isotypic with $CdTm_4Mo_3O_{16}$ [19]. The refined atomic coordinates after the refinement are listed in Table 1, and the bond distances and angles are given in Table 2.

A representation of the crystal structure is shown in Fig. 3. The oxygen coordination polyhedra for Pr1, Pr2 and Mo are shown in Fig. 4. Both Pr atoms are coordinated to eight oxygen atoms, within rather distorted scalenohedra. For $Pr1O_8$ the polyhedron contains 4 Pr1–O1 bond lengths of 2.589(4) Å, and 4 Pr1–O2 of 2.380(4) Å with average ⟨Pr–O⟩ distances of 2.485 Å; in $Pr2O_8$ there are 6 Pr2–O1 bond lengths of 2.619(2) Å and 2 Pr2–O2 distances of 2.311(3) Å, with a ⟨Pr2–O⟩ average of 2.542 Å. We can define the relative distortion of the polyhedra with the Δ_d parameter, concerning the deviation of Pr–O distances with respect to the average ⟨Pr–O⟩ value, as $\Delta_d = (1/8)\sum_{n=1,8}[(d_n - \langle d \rangle)/\langle d \rangle]$ [2]; we obtain $\Delta_d(Pr1) = 17.7 \times 10^{-4}$ and $\Delta_d(Pr2) = 27.7 \times 10^{-4}$. Mo atoms are bonded to four oxygen atoms at distances of 1.788(2) Å conforming quasi-regular tetrahedral units (O–Mo–O angles are 116.3(2)° and 106.2(2)°). A description of the structure can be obtained from Fig. 5. $Pr1O_8$ scalenohedra form trimer units by sharing three edges via O2 atoms; every two of these units form a quasi-cubic cavity where Pr2 atoms are located; thus the $Pr2O_8$ scalenohedron shares three edges

Table 2
Main bond distances (Å) and selected angles (deg.) for $Pr_5Mo_3O_{15}$ determined from NPD data at RT.

Pr1–O1 (× 4)	2.589(4)
Pr1–O2 (× 4)	2.380(4)
Pr2–O1 (× 6)	2.619(2)
Pr2–O2 (× 2)	2.311(3)
Mo–O1 (× 4)	1.788(2)
O1–Mo–O1 (× 2)	116.3(2)
O1–Mo–O1 (× 2)	106.2(2)

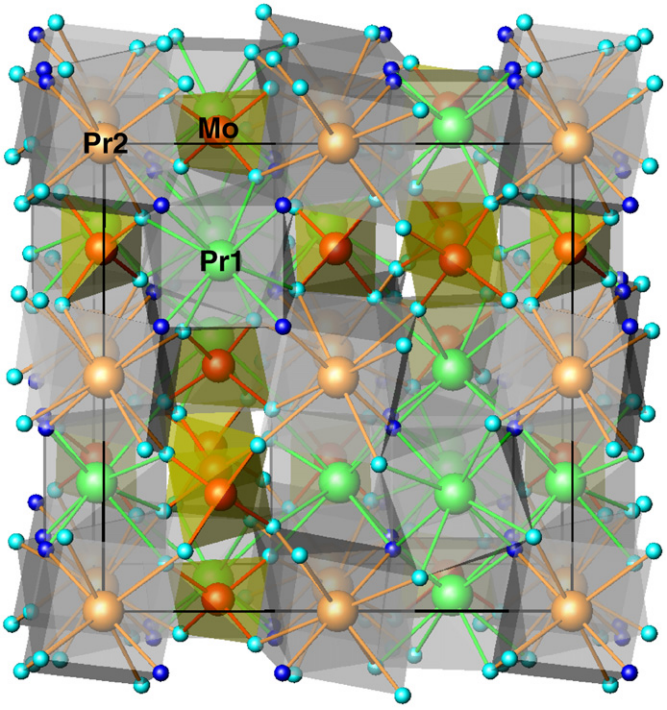

Fig. 3. View of the crystal structure of $Pr_5Mo_3O_{16}$ along an axis: PrO_8 scalenohedra are long-range ordered with MoO_4 tetragonal units.

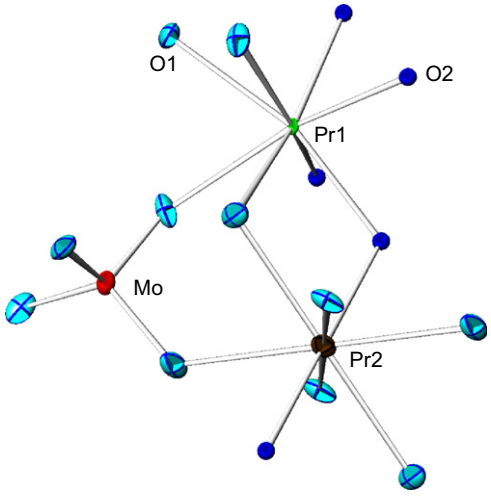

Fig. 4. ORTEP plot of the asymmetric unit of $Pr_5Mo_3O_{16}$, showing the oxygen coordination of Pr1, Pr2 and Mo.

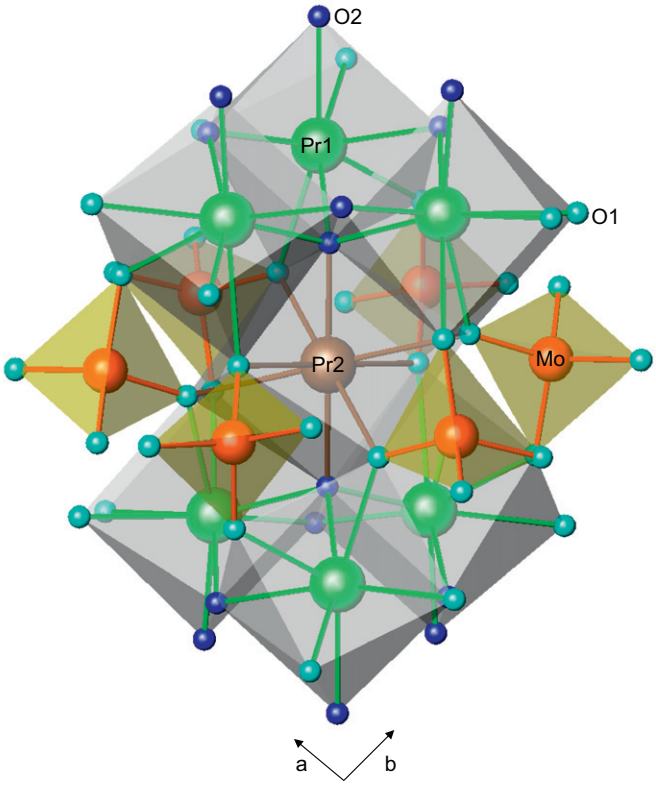

Fig. 5. Partial view of the crystal structure of $Pr_5Mo_3O_{16}$; $Pr1O_8$ scalenohedra share three edges forming a quasi-cubic cavity where Pr2 atoms are located; the MoO_4 tetrahedra are corner connected to both Pr scalenohedra.

with the upper Pr_3O_{19} unit and three edges with the lower unit. The MoO_4 tetrahedra are bridging the upper and lower units, by sharing corners via the O1 oxygen. The MoO_4 tetrahedra are isolated from each other (they do not share common oxygen), forming discrete units.

It is simple to understand the relationship of this complex superstructure with the basic fluorite CaF_2 structure, containing regular CaF_8 units in a cubic coordination. The unit-cell parameters of the cubic structure of $Pr_5Mo_3O_{16}$ are related with the simple cubic a_f fluorite unit cell as $a \approx 2a_f$ (a_f=5.5 Å). $Pr_5Mo_3O_{16}$ can be rewritten as M_8O_{16}, containing 8 fluorite MO_2 units per formula and 32 MO_2 units per unit cell. The complex cubic superstructure thus results from the long-range ordering between PrO_8 and MoO_4 polyhedra across the crystal. In the fluorite structure every CaF_8 cubic polyhedron shares edges with 8 neighboring units. In $Pr_5Mo_3O_{16}$ this long-range arrangement is perturbed by the presence of MoO_4 tetrahedra, corner linked with 4 neighboring PrO_8 units. It is important to highlight that this structural type does not contain oxygen vacancies (as it happens in many fluorite-like oxygen-defective oxides, such as Pr_6O_{11}, deriving from PrO_2 by removal of 1/12 of the anions [20]). In the present case, the strong preference of Mo for the tetrahedral coordination gives rise to a deformation of the oxygen sublattice, inducing the presence of cavities adjacent to the MoO_4 tetrahedra, as it is highlighted in Fig. 6. These cavities could provide an easy diffusion path for oxygen ions, via interstitial positions, which is certainly worth exploring; the oxygen transport properties of this material have not been reported up to date.

It is interesting to get an insight into the valence states of the different cations present in the solids by means of the Brown's bond valence model [21,22]. It gives a phenomenological relationship between the formal valence of a bond and the corresponding bond length. Table 3 includes the valences calculated for Pr, Mo and O

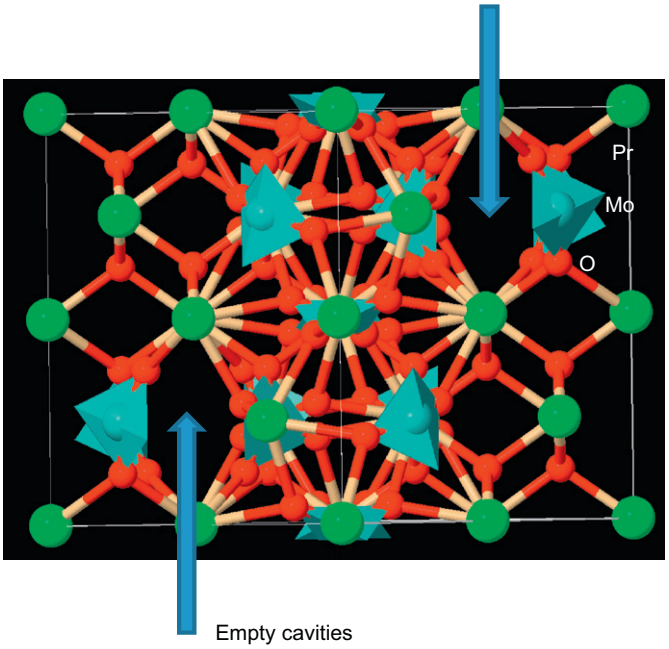

Fig. 6. [1 1 0] projection of the crystal structure, highlighting the presence of cavities adjacent to the MoO_4 tetrahedra.

Table 3
Valences[a] determined from the individual Pr–O and Mo–O distances in $Pr_5Mo_3O_{16}$.

Pr1	3.26(1)
Pr2	2.887(9)
Mo	5.52(2)
O1	1.947(9)
O2	2.19(1)
GII	0.277

[a] The valence is the sum of the individual bond valences (s_i) for Pr–O and Mo–O bonds. Bond valences are calculated as $s_i=\exp[(r_0-r_i)/B]$; $B=0.37$, $r_0=1.743$ for the Mo^{6+}–O^{2-} pair and $r_0=2.135$ for the Pr^{3+}–O^{2-} pair, from Ref. [22]. Individual Pr–O and Mo–O distances (r_i) are taken from Table 2. The global instability index (GII) is calculated as the root mean of the valence deviations for the $j=1, \ldots, N$ atoms in the asymmetric unit, according to $GII=(\Sigma_j[\Sigma_i(s_{ij}-V_j)^2]/N)^{1/2}$.

from the individual Pr–O and Mo–O distances in $Pr_5Mo_3O_{16}$. The valence of Pr1 ions is significantly higher than the expected value of +3 whereas the valence of Pr2 atom is slightly lower than +3. This result suggests that Pr1 atoms are overbonded while Pr2 are slightly underbonded in this structure; in other words Pr1–O bonds are, in average, under compressive stress and Pr2–O bonds are under tensile stress, giving rise to a structure with a slight instable character. The variability of oxidation states observed for Pr, able to adopt trivalent and tetravalent states with easiness can account for the clear deviation of Pr2 to an overbonded state. On the other hand, the valence of Mo ions is 5.5, noticeably below the 6+ oxidation state commonly found in many molybdates (for instance, $CaMoO_4$ with scheelite structure). Probably, the size of the tetrahedral coordination environment for Mo, conformed by the surrounding PrO_8 polyhedra in the fluorite substructure, is too large to allow Mo to satisfy its bonding requirement and to reach the hexavalent state. The fact that MoO_4 tetrahedra are isolated in this structure, having no common oxygen, prevents the electronic delocalization across the structure, since otherwise the intermediate valence state of Mo would lead to a black-colored compound with electronic conductivity. Transport measurements in sintered pellets show that $Pr_5Mo_3O_{16}$ is insulating at room temperature, with resistivities higher than $10^8\,\Omega\,cm$. The variation of the electrical resistance with temperature was not measured.

The charge distribution observed in $Pr_5Mo_3O_{16}$ is different from that obtained in other members of this structural family, $CdTm_4Mo_3O_{16}$ [19] and $CdY_4Mo_3O_{16}$ [23]. In these Cd-containing compounds, Cd and $R=Y$, Tm are occupying randomly the 8*c* sites (average oxidation state of 2.5+), whereas the 12*e* positions are uniquely occupied by R^{3+}, and Mo is, nominally, hexavalent. In the present case, Mo clearly exhibits a reduced oxidation state close to $Mo^{5.5+}$, whereas the bond valence obtained for Pr1 indicates a mixed Pr^{3+}–Pr^{4+} state, perhaps suggesting a partial charge disproportionation effect between Pr and Mo. An assumption of a purely trivalent Pr in $Pr_5Mo_3O_{16}$ would give a nominal valence of 5.67+ for molybdenum.

The presence of structural stresses in the crystal structure can be quantified by means of the "Global Instability Index" [24], GII in Table 3, which is calculated from the differences between observed and expected valences for all the atoms in the asymmetric unit. It is a measure of the extent to which the BVS rule is violated over the whole structure. As suggested by Brown [24] and Armbruster et al. [25], GII values higher than 0.2 v.u. indicate the presence of intrinsic strains large enough to cause instability at room temperature. In the present case GII is 0.28 indicating a noticeable structural instability. This fact perhaps accounts for the stabilization of different crystal structures for other rare earths such as the α-R_2MoO_6 polytype, stable for R=Tb,…, Yb [14,16], or the γ polytype for La_2MoO_6.

Finally, it is worth extending the present results to the compound of nominal composition Ce_2MoO_6. As commented above, the similarity of the XRD diagrams of both oxides, including the superlattice reflections, suggests that both materials are isostructural, implying that the true composition of the Ce oxide may indeed be $Ce_5Mo_3O_{16}$. A study by X-ray spectroscopy of this material [4] already gave some insight on the coordination of the metal ions, in particular a distorted $Ce–O_8$ coordination environment and the tetrahedral location of the Mo ions. However, the description of Ce_2MoO_6 with trivalent cerium and hexavalent Mo was inconsistent with previously proposed charge transfer models [15,26,27]. Moreover, as recognized by the authors of Ref. [4], the X-ray spectroscopy results lead to a quandary about the structure of Ce_2MoO_6, difficult to rationalize with a Ce^{3+}/Mo^{6+} cation distribution. The present structural model for $Pr_5Mo_3O_{16}$, extrapolated to the Ce isomorph, could justify a Ce mixed valence, the presence of Mo in a reduced oxidation state and, plausibly, the occurrence of an internal charge transfer implying the reduction of Mo^{6+} by Ce^{3+} accounting for the unusual electronic properties of this material.

4. Conclusions

The β-R_2MoO_6 polymorph has been investigated for R=Pr. The crystal structure, refined from NPD data, indeed corresponds to a $Pr_5Mo_3O_{16}$ stoichiometry. It is a cubic superstructure of fluorite, formed by the long-range ordering of PrO_8 and MoO_4 coordination polyhedra. The two kinds of PrO_8 scalenohedra share common edges and are interconnected by MoO_4 tetrahedra by sharing corners with them. A bond-valence study indicates that the charge distribution observed in $Pr_5Mo_3O_{16}$ is different from that obtained in other members of this structural family, such as $CdTm_4Mo_3O_{16}$, containing hexavalent molybdenum. In the present case, Mo ions clearly exhibit a reduced oxidation state close to $Mo^{5.5+}$, whereas the bond valence obtained for Pr1 indicates a mixed Pr^{3+}–Pr^{4+} state, perhaps suggesting a partial charge disproportionation effect between Pr and Mo. Given the similarity of the XRD pattern of $Pr_5Mo_3O_{16}$ with that published for Ce_2MoO_6, it can be assumed that this latter oxide also

exhibits an analogous crystal structure and charge distribution, which needs to be further proved experimentally.

Acknowledgments

We thank the financial support of the Spanish Ministry of science and Innovation to the project MAT2007-60536. This work was partially performed at the spallation source SINQ, Paul Scherrer Institute, Villigen, Switzerland.

References

[1] C.N.R. Rao, B. Raveau, Transition metal oxides, VCH Publishers, New York, 1995.
[2] C.N.R. Rao, B. Raveau (Eds.), World Scientific Publishing, Singapore, 1998.
[3] J.M. Thomas, W.J. Thomas, Principles and practice of heterogeneous catalysis, VCH Publishers, Weinheim, 1997.
[4] M.R. Antonio, U. Staub, J.S. Xue, L. Soderholm, Chem. Mater. 8 (1996) 2673.
[5] F.P. Netzer, E. Bertel, in: K.A. Gschneidner, L. Eyring (Eds.), Handbook Physics and Chemistry of Rare Earths, Vol. 5, Amsterdam, North Holland1982, pp. 217–320.
[6] J.F. Brazdil, in: I.E. Wachs, L.E. Fitzpatrick (Eds.), Characterization of Catalytic Materials, Butterworth-Heinemann, Boston1992, pp. 47–68.
[7] J.M. Lopez Nieto, J.L.G. Fierro, L. Gonzalez Tejuca, G.J. Kremenic, Catalysis 107 (1987) 325.
[8] G. Kremenic, J.M. Lopez Nieto, J.M.D. Tascon, L. Gonzalez Tejuca, S.W. Weller, Ind. Eng. Chem. Res. 26 (1987) 1419.
[9] G. Kremenic, J.M. Lopez Nieto, J.M.D. Tascon, L. Gonzalez Tejuca, J. Less Comm. Met. 138 (1988) 47.
[10] G. Kremenic, J.M. Lopez Nieto, J.M.D. Tascon, L. Gonzalez Tejuca, J. Less Comm. Met. 135 (1987) 95.
[11] F. De Smet, P. Ruiz, B. Delmon, M. Devillers., J. Phys. Chem. B 105 (2001) 12355.
[12] F. De Smet, P. Ruiz, B. Delmon, M. Devillers, Appl. Catal. A—General 172 (1998) 333.
[13] F. De Smet, M. Devillers, C. Poleunis, P. Bertrand, J. Chem. Soc. Faraday Trans. 94 (1998) 941.
[14] J.S. Xue, M.R. Antonio, L. Soderholm, Chem. Mater. 7 (1995) 333.
[15] L.H. Brixner, Rev. Chim. Miner. 10 (1973) 47.
[16] J.A. Alonso, F. Rivillas, M.J. Martínez-Lope, V. Pomjakushin, J. Solid State Chem. 177 (2004) 2470.
[17] V. Favre-Nicolin, R. Černý, J. Appl. Crystallogr. 35 (2002) 734.
[18] J. Rodríguez-Carvajal, Physica B 192 (1993) 55.
[19] J.P. Faurie, R. Kohlmuller, Rev. Chim. Miner. 8 (1971) 241.
[20] A.F. Wells, in: Structural Inorganic Chemistry, 5th edn., Clarendon Press, Oxford, 1984, pp. 543.
[21] I.D. Brown, Structure and Bonding in Crystals, in: M. O'Keefe, A. Navrotsky (Eds.), Academic Press, New York1981, p. 1 vol.2.
[22] N.E. Brese, M. O'Keefe Acta, Crystallogr. Sect. B 47 (1991) 192.
[23] J.B. Bourdet, R. Chevalier, J.P. Fournier, R. Kohlmuller, J. Omaly, Acta Crystallogr. B 38 (1982) 2371.
[24] I.D. Brown, Z. Kristallogr. 199 (1992) 255.
[25] T. Armbuster, F. Röthlisberger, F. Seifer, Am. Mineral. 75 (1990) 847.
[26] L.H. Brixner, A.W. Sleight, M.S. Licis, J. Solid State Chem. 5 (1972) 186.
[27] A. Manthiram, J. Gopalakrishnan, J. Less-Common Met. 99 (1984) 107.